A Detailed Investigation on the Convective Heat Transfer Inside the Enclosed Cavity of Insulated Glass Solar Thermal Flat-Plate Collectors

Thorsten Summ, Mohannad Abdalsalam, Mathias Ehrenwirth, Christoph Trinkl and Wilfried Zörner

Institute of new Energy Systems (InES), Technische Hochschule Ingolstadt, Ingolstadt (Germany)

Abstract

In the solar thermal industry, there is a trend towards large-scale solar district heating plants. However, building large plants can also lead to problematic fluctuations in demand for collector manufacturers. To tackle this issue, an innovative concept was introduced which adapts the collector design to production techniques of the insulating glass industry. The insulated glass solar thermal flat-plate collector (IGFPC) raises new questions regarding efficiency and convective heat losses. The objective of this research was to determine the natural convection characteristics of this collector design. A review of Nusselt number correlations revealed, that the gas cavity of the collector can be partially described using equations from literature. As these equations do not consider both large aspect ratios and higher temperature levels, a computational fluid dynamics simulation was performed. The results show that convective heat transfer inside IGFPCs occurs predominantly in front of the absorber, whereas inside the rear cavity the flow patterns are subcritical, resulting in smaller convective losses. As a consequence, the absorber of this collector should be positioned asymmetrically in order to minimize its convective losses. A new set of Nusselt correlations has been derived to express the heat transfer characteristics for typical operating ranges of IGFPCs and various inclination angles.

Keywords: solar thermal collector, flat-plate collector, insulated glass, convective heat losses, natural convection, computational fluid dynamics, solar district heating, Nusselt correlations, Rayleigh number, inclination angle

1. Introduction

As global temperature rises, the need for achieving the climate targets within all sectors of our society is a must. It's noted that most of the carbon dioxide emissions in the northern hemisphere are related to electricity and heating processes (World Resources Institute, 2019) where specifically, heating has the biggest share of overall energy consumption in European households (Eurostat, 2018). Many leading countries have proven that large-scale district heating plants based on solar thermal resources can be operated both efficiently and profitable (Tschopp et al., 2020). However, large solar thermal projects may cause high fluctuations in demand, resulting in financial challenges for collector manufacturers (REN21 Secretariat, 2020).

A solution to tackle such a problem is to redesign the solar thermal flat-plate collectors (FPCs) in a way that can lower the manufacturing cost without losing too much of overall efficiency. One approach to achieve this, is the concept of insulated glass solar thermal flat-plate collectors (IGFPCs) which were studied by different researchers in the last years (Giovannetti et al., 2014; Giovannetti and Kirchner, 2015; Leibbrandt et al., 2017; Leibbrandt and Schabbach, 2020; Leibbrandt et al., 2022). What sets this collector apart is the idea of fixing the absorber between two glass panels, as seen in Fig. 1. Using a manufacturing technique similar to insulated double-glazed units allows for the injection of noble gas into the collector cavity, which reduces thermal losses. A polymeric adhesive at the glass edges ensures both the hermetic sealing of the gas cavity and the mechanical stability of the assembly.

Convective losses through the cavity between the glazing and the absorber represent the dominant part of heat losses in flat-plate collectors. Hence, the phenomenon is discussed as early as the 1950s (de Graaf, J. G. A. and van der Held, 1953). The lack of insulation material at the back side IGFPC increases the share of

doi:10.18086/swc.2021.22.09 Available at http://proceedings.ises.org

convective and radiative losses. Throughout the years, many researchers studied factors which affect the thermal energy transfer through the cavity as glazing type, cavity medium and aspect ratio. Moreover, many researchers developed correlations that determine the convective losses between absorber and the frontside glazing of an FPC.

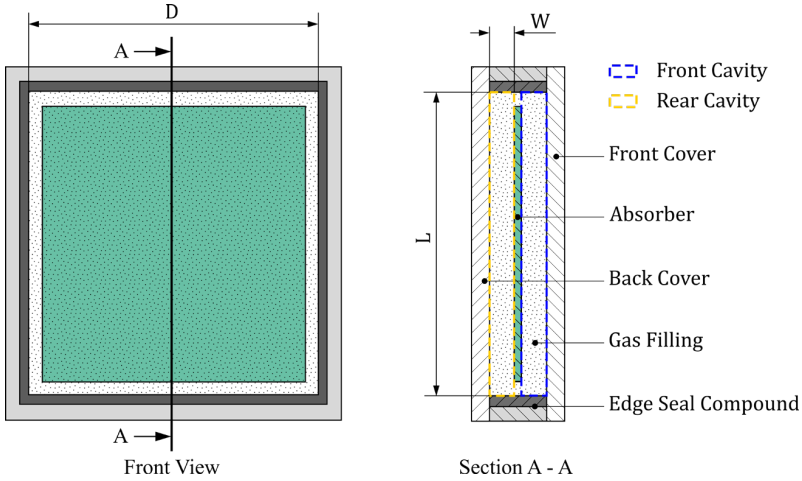

Fig. 1: Schematic and simplified structure of an IGFPC consisting of two glass covers, an absorber plate and an edge seal compound. Inlet and outlet ports are not drawn for reasons of simplicity.

In order to fully assess the potential of IGFPCs, an investigation on the convective heat losses of IGFPCs with regard to both cavities was made in this present study. The losses in the rear cavity were not investigated with regard to IGFPCs. The presented article focuses on the convective heat losses of such collectors by analyzing both front and rear cavities. The objective of this research is to determine the convective heat transfer characteristics of such a configuration by reviewing former applicable findings and verifying the results with numerical flow simulations.

2. Methodology

2.1 Review of empirical Nusselt correlations

As shown in an earlier investigation (Summ et al., 2020), the front and back side of the IGFPC may be considered as two separated cavities. Heat losses that occur at the side boundaries can be neglected. There are two arguments to justify this assumption. Firstly, the thickness of a large-area collector (LAC) is several orders of magnitude smaller than the collector length or width. Secondly, the material used in the edge seal compound of the IGFPC holds significantly lower thermal conductivity than the materials used in conventional collectors. Condensing the losses in such a way allows for the application of well-known equations in order to describe the convective heat losses of the IGFPC.

In order to give an overview of the existing methods for calculating the convective heat losses of IGFPCs, an investigation on empirical expressions describing rectangular cavities was conducted (cf. chapter 3.1). Natural convective heat transfer is typically quantified in terms of Nusselt number (Nu) which significantly depends on Rayleigh number (Ra) and the inclination angle of the cavity (φ). These expressions (also called correlations), were later (cf. chapter 3.3) used to compute the heat transfer coefficient (h) by applying the definition of Nusselt number:

$$h = \frac{Nu(Ra, \varphi)\, k}{W} \qquad \text{(eq. 1)} \qquad k\text{: thermal conductivity of the gas inside the cavity}$$

2.2. Computational fluid dynamics simulation setup

The correlations given in the literature cannot be applied for the entire spectrum of geometrical and operating properties that are relevant for the design of IGFPCs. Additionally, since many correlations exist, it is worth finding the most accurate one which can describe the convective losses for this particular collector concept. In this context, computational fluid dynamics (CFD) simulations of the described cavities were performed. Typical boundary conditions for LACs used for district heating applications were incorporated. The CFD

model was compared and validated with the empirical results of other authors (cf. chapter 2.3 / 3.2).

As described in chapter 1, the cavity is modelled as a cuboid and has the dimensions of $L \times W \times D$ (length, width, and depth). The model uses a symmetry boundary condition to the cross-section plane (cf. Fig. 1) to reduce the computational effort, resulting in a fluid domain with the size $L \times W \times \frac{D}{2}$.

To provide a structured mesh and therefore numerical stability as well as computational speed, a mesh with hexagonal elements was created. Size functions have been used to create refinements at the walls and to resolve boundary layer effects. The number of edge divisions was varied for each side of the geometry. The selected parameters are listed in Tab. 3. Consequently, a cell count of roughly two million elements was set. The mesh needed adaptation after validating the model, as the aspect ratio ($AR = L/W$) was up to 10 times higher for the parametric study. The width and length of the cavity were changed and hence, the mesh refinements too.

The CFD simulation was performed using ANSYS Fluent 2020R2 software (ANSYS, Inc., 2020). A steady-state, pressure-based finite volume approach was selected to solve the Navier-Stokes equations numerically. The Reynolds stress turbulence model was used to account for high Rayleigh numbers, turbulent flow regimes and turbulent boundary layer effects.

The physics of natural convection require the gas properties to be temperature dependent. Therefore, the ideal gas law and kinetic theory were used to compute density, thermal conductivity, viscosity, and heat capacity of the gas. The parameters for the used gases Air and Argon are listed in Tab. 4. In this study, the CFD computation was validated using Air as a cavity gas. However, an analytical computation accounting for Argon was conducted as well (cf. chapter 3.3).

The boundary conditions were applied to four regions: a constant temperature at the surfaces representing the absorber and the front/back glass cover; an adiabatic condition at the side walls; a symmetry condition at the cross-section plane. The inclination was varied by changing the components of the gravity vector using the following expressions: $g_x = g \sin\varphi$ and $g_z = -g \cos\varphi$, where $g = 9.81\ \mathrm{m\ s^{-2}}$.

Output parameters from the Fluent model were the heat flow rate $\dot{Q}$, Rayleigh and Nusselt numbers which were computed using their common definitions:

$$Nu = \frac{h\,W}{k} = \frac{\dot{Q}\,W}{k\,L\,\frac{D}{2}\,\Delta\mathrm{T}} \qquad \text{(eq. 2)} \qquad\qquad Ra = \frac{g\,\Delta T\,W^3\,\rho\,c_p}{\nu\,T_{gas}\,k} \qquad \text{(eq. 3)}$$

ΔT: temperature difference ρ: mass density c_p: heat capacity ν: kinematic viscosity T_{gas}: gas temperature

2.3 Validation of the CFD model with empirical findings

The collected equations from the literature have been used for validating the numerical model. Not all equations are valid for the entire range of Ra and φ. However, the collection of correlations covers the range for this study to a high degree. The parameters were selected in such a way that most of the equations could be used to compute values for Nu.

Thus, the computation was performed for the inclination angles $\varphi = \{0, 15, 30, 45, 60\}^{\circ}$ as well as for Rayleigh numbers $Ra = \{10^3, 5\times10^3, 10^4, 5\times10^4, 10^5\}$. Several values for ΔT were selected in order to achieve the four stated levels of Ra and were respectively $\Delta\mathrm{T} = \{0.571, 2.858, 5.717, 28.583, 57.165\}$ K. More details on the geometrical setup are described in Tab. 3. For validation, isothermal boundary conditions were used for the front cover and the absorber. To validate the model, the results from the correlations were then compared to the simulation outputs by means of Nu vs. Ra plots.

2.4 Parametric study using the CFD model

To analyze the collector characteristics, a parametric study was conducted. The width of the cavity (W) and the angle (φ) were used as geometric parameters, whereas the temperature difference (ΔT) was varied as a parameter related to the operating point of the collector. A constant length of $L = 2.5$ m and depth $D = 1.5$ m was implemented, accounting for the larger sizes of IGFPCs as compared to the geometry for validation.

As described in chapter 2.1, the front and back side of the absorber were computed separately. Eismann (2015) found in his investigation on the convective losses of FPCs, that the inhomogeneous temperature distribution

across the absorber is relevant for computing the thermal losses. Therefore, in this study the boundary conditions of the absorber were set to be non-isothermal as well. A negative linear temperature gradient along the absorber plate was applied to this boundary in order to account for an inhomogeneous temperature field. At both ends of the absorber, the temperature is set to be the inlet and outlet temperature of the heat transfer fluid[1]. The side walls of the geometry were defined as adiabatic and the boundary for the glass cover was defined as isothermal.

For the parametric study, inlet, outlet, and glass temperature were varied. This leads to a set of different Rayleigh numbers. During operation, solar thermal collectors can have various temperature distributions. To cover a realistic range of operation modes, four sets of parameters have been defined. Tab. 1 shows the four parameter sets that were used for the CFD computations. Additionally, the inclination angle (φ), and cavity width (W) were altered as: $\varphi = \{10, 40, 70, 110, 140, 170\}^{\circ}$ and $W = \{5, 16.25, 27.5, 38.75, 50\}$ mm. This results in a total number of 125 simulations for the parametric study. Here, φ and W were selected to cover a broad range of realistic operating and design characteristics. Linear spacing was used for W to have five equally spaced parameters between 5 mm and 50 mm.

3. Results and Discussion

3.1 Review of empirical approaches

The heat transfer across the gas layer of enclosed cavities has been studied very thoroughly. Researchers identified mathematical correlations for different physical boundary conditions such as temperature level, cavity dimensions or gas types. Within the presented study, a collection of correlations has been obtained describing the convective heat transfer across rectangular shaped enclosed cavities. Investigations that only covered low aspect ratios (< 8) or a Prandtl number (Pr) range for liquids or other types of geometries have not been included in the collection. Tab. 2 shows the correlations as well as their specific validity range. Some of these equations can be applied to the back side of the collectors as well, such as the ones from Ayyaswamy and Catton (1973), Ozoe et al. (1975), and ElSherbiny (1996).

As this type of collector shall be used for district heating applications, these assumptions were made:

- The inlet temperature T_i of the collector ranges from 10 °C to 70 °C
- The outlet temperature T_o of the collector ranges from 20 °C to 120 °C
- The temperature spread $S = T_o - T_i$ between inlet and outlet ranges from 0 K to 50 K
- The ambient temperature T_a ranges from -10 °C to 30 °C
- The inclination angle φ of the collector ranges from 10° to 70°
- The average collector temperature is $T_m = 0.5\ (T_o + T_i)$
- The average glass cover temperature is $T_{gl} = 0.5\ (T_m + T_a)$
- The average cavity gas temperature is $T_{gas} = 0.5\ (T_m + T_{gl})$

These considerations given, the operating temperature difference $\Delta T_c = T_m - T_a$ for IGFPCs ranges between -15 K and 105 K. As the presented work is aimed in the convective losses only, the values $\Delta T_c < 0$ K were neglected. Hence, the front and back cover will have higher or equal temperatures than ambient. For a computation of the Rayleigh and Nusselt numbers, we define the temperature difference as $\Delta T = T_m - T_{gl}$. The aforementioned temperatures yield ΔT between 0 K and 52.2 K and average gas temperatures T_{gas} between 8.75 °C and 78.75 °C.

Within this study, the investigated IGFPC has a length of $L = 2.5$ m and a depth of $D = 1.5$ m. Since the cavity width W will affect Rayleigh number and therefore the heat losses, this parameter is an important design measure. It is assumed to vary from 5 mm to 50 mm both at the front and the back side of the absorber. The aspect ratio of the cavity AR will therefore range from 50 to 500. It has been shown by Inaba (1984), that for large aspect ratios the dependence of Nu to AR will become negligible. However, the existing correlations are

[1] In the model, no heat transfer fluid (HTF) is included. The temperature is referring to the HTF that would have effect on the absorber temperature during a real operation of the collector.

not depicted to have validity for such large aspect ratios (cf. Tab. 2). The frequently cited work from Hollands et al. (1976) is valid for $Ra \leq 10^5$ and $AR = 48$. None of the applicable correlations from literature will exceed aspect ratios of 100. Considering all these assumptions and definitions, we obtain a Rayleigh number range as $Ra < 3.2 \times 10^5$ for this study.

Tab. 1: The selected set of parameters that were used for the parametric study

No.	T_i [°C]	T_o [°C]	T_{gl} [°C]	ΔT [K]	S [K]	ΔT_c [K]	T_m [°C]	T_{gas} [°C]
1	40	70	42.5	12.5	30	25	55	48.75
2	60	110	57.5	27.5	50	55	85	71.25
3	70	80	32.5	42.5	10	85	75	53.75
4	70	110	40.0	50.0	40	100	90	65.00

Tab. 2: Collection of Nusselt correlations from the literature[1]

Reference	Nu-Ra-Correlation	φ in °	Ra / Ra_φ / Gr	AR
de Graaf, J. G. A. and van der Held, 1953	$Nu = C\ Gr^n$ Various values for C and n depending on φ and Gr	0, 20, 30, 45, 60, 70, 90	$2 \times 10^3 < Gr < 2 \times 10^5$	18.8 34.1 62.3
Ayyaswamy and Catton, 1973	$Nu = Nu_{90°}\,[\sin\varphi]^{0.25}$	$70 < \varphi < 120$	$Ra\ AR^3 \sin\varphi \gg 10^4$	$AR \gg \cot\varphi$
Ozoe et al., 1975	$Nu = 0.109\ Ra_\varphi{}^{1/3}$	"small angles"	$10^3 < Ra < 10^5$	8.4 15.5
Hollands et al., 1976	$Nu = 1 + 1.44\left[1 - \frac{1708}{Ra_\varphi}\right]^+ \left[1 - \frac{1708\,(\sin(1.8\varphi))^{1.6}}{Ra_\varphi}\right] + \left[\left(\frac{Ra_\varphi}{5830}\right)^{1/3} - 1\right]^+$	$0 \leq \varphi \leq 60$	$0 \leq Ra \leq 10^5$	48
Buchberg et al., 1976	$Nu = 1 + 1.446\left[1 - \frac{1708}{Ra_\varphi}\right]^+$ $1708 < Ra_\varphi < 5900$ $Nu = 0.229\ Ra_\varphi^{0.252}$ $5900 < Ra_\varphi < 9.2 \times 10^4$ $Nu = 0.157\ Ra_\varphi^{0.285}$ $9.2 \times 10^4 < Ra_\varphi < 10^6$	$0 \leq \varphi \leq 60$	$1708 < Ra_\varphi < 10^6$	–
Randall et al., 1979	$Nu = 0.118\ Ra \cos\varphi - 4520.29$	$45 \leq \varphi \leq 90$	$2.8 \times 10^3 < Ra < 2.2 \times 10^5$	$9 - 36$
Schinkel, 1980	$Nu = C\ Ra^{1/3}$ $\varphi = 0°\ C = 0.080$ | $\varphi = 10°\ C = 0.079$ $\varphi = 20°\ C = 0.075$ | $\varphi = 30°, 40°, 50°\ C = 0.074$ $\varphi = 60°\ C = 0.072$ | $\varphi = 70°\ C = 0.069$ $\varphi = 80°\ C = 0.068$ | $\varphi = 90°\ C = 0.062$	$0 \leq \varphi \leq 90$	$10^5 < Ra < 4 \times 10^6$	$6 - 27$
Inaba, 1984	$Nu = 1 + 1.21\left(1 - \frac{2500}{Ra_\varphi}\right)$ $2.5 \times 10^3 < Ra_\varphi < 6 \times 10^3$ $Nu = 0.199\ Ra_\varphi^{0.258}$ $6 \times 10^3 < Ra_\varphi < 4 \times 10^5$ $Nu = 0.0785\ Ra_\varphi^{0.330}$ $4 \times 10^5 < Ra_\varphi < 1.2 \times 10^6$ $Nu = 0.271\ AR^{-0.21}(Ra \sin\varphi)^{0.25}$ $5 \times 10^3 < Ra \sin\varphi < 1.2 \times 10^6$ and $60 < \varphi \leq 120$	$0 \leq \varphi \leq 120$	$2.5 \times 10^3 < Ra < 1.2 \times 10^6$	$5 - 83$
ElSherbiny, 1996	$Nu_{180} = [1 + (0.212\ Ra^{0.136})^{11}]^{1/11}$ $Nu_{120} = [1 + (0.0566\ Ra^{0.332})^{4.76}]^{1/4.76}$ $Nu = Nu_{180} + \frac{180-\varphi}{60}(Nu_{120} - Nu_{180})$	$120 \leq \varphi \leq 180$	$10^2 < Ra < 2 \times 10^6$	20
Matuska and Zmrhal, 2009	$Nu = (0.1464 - 2.602 \times 10^{-4}\ \varphi - 2.046 \times 10^{-6}\ \varphi^2)\ Ra^{0.29}$	$0 \leq \varphi \leq 90$	$10^4 \leq Ra \leq 2 \times 10^6$	–
Eismann, 2015	$Nu = 1 + Nu_1 + Nu_2$ $Nu_1 = 1.44\left(1 - \frac{1708}{Ra + 1708\,R_c}\right)\left[1 - (\sin(1.8\,\varphi))^{1.6}\frac{1708}{Ra + 1708\,R_c}\right]$ $Nu_2 = \left[\left(\frac{Ra + 5830\,R_c}{5830}\right)^{0.39} - 1\right](1 + C\,R_c)$	–	$10^3 \leq Ra \leq 10^6$	–

[1] Superscript $[]^+$ indicates that only positive values will be counted as $[A]^+ = 0.5[abs(A) + A]$

IGFPCs are expected to work efficiently when Argon is filled in the enclosed cavity between the front and back glass pane. Due to its lower thermal conductivity, the gas causes lower convective heat losses compared to an air-filled cavity. Since the thermodynamic properties of Argon are different to the ones of Air, the resulting Rayleigh number for the same state of collector operation is higher. With respect to the values computed above, Ra is up to 3.70×10^4 higher when Argon is filled inside the cavity. This effect has to be accounted for when designing IGFPCs. Argon and Air have different Prandtl numbers. However, authors have found that Nusselt number is independent of Pr which is why most of the correlations do not account for Pr.

3.2 Validation results

The Nusselt-Rayleigh relation is shown in Fig. 2 for the five inclination angles $0°, 15°, 30°, 45°$ and $60°$. A majority of the curves follow the frequently cited equation from Hollands. However, not all curves can be drawn for each plot, as the range of validity is exceeded in some cases. The correlation from Eismann (2015) shows a significant deviation from the others. However, most curves diverge slightly with increasing Ra. The differences increase with greater inclination angles.

The CFD model shows a good fit for the correlations from Tab. 2. For higher Rayleigh numbers, the computed Nusselt numbers deviate slightly from the majority of curves and match closer to the equation from Eismann (2015). Overall, the simulated set of parameters is in good agreement to the empirical results collected in the last decades. Given this agreement, it can be concluded that the CFD model is able to describe the physical effects of the heat transfer well. Even for $Ra_\varphi > Ra_c = \{1708, 5830\}$ when the flow is characterized by convective rolls (cf. Hart (1971)), the model is capable of computing the heat transfer accurately.

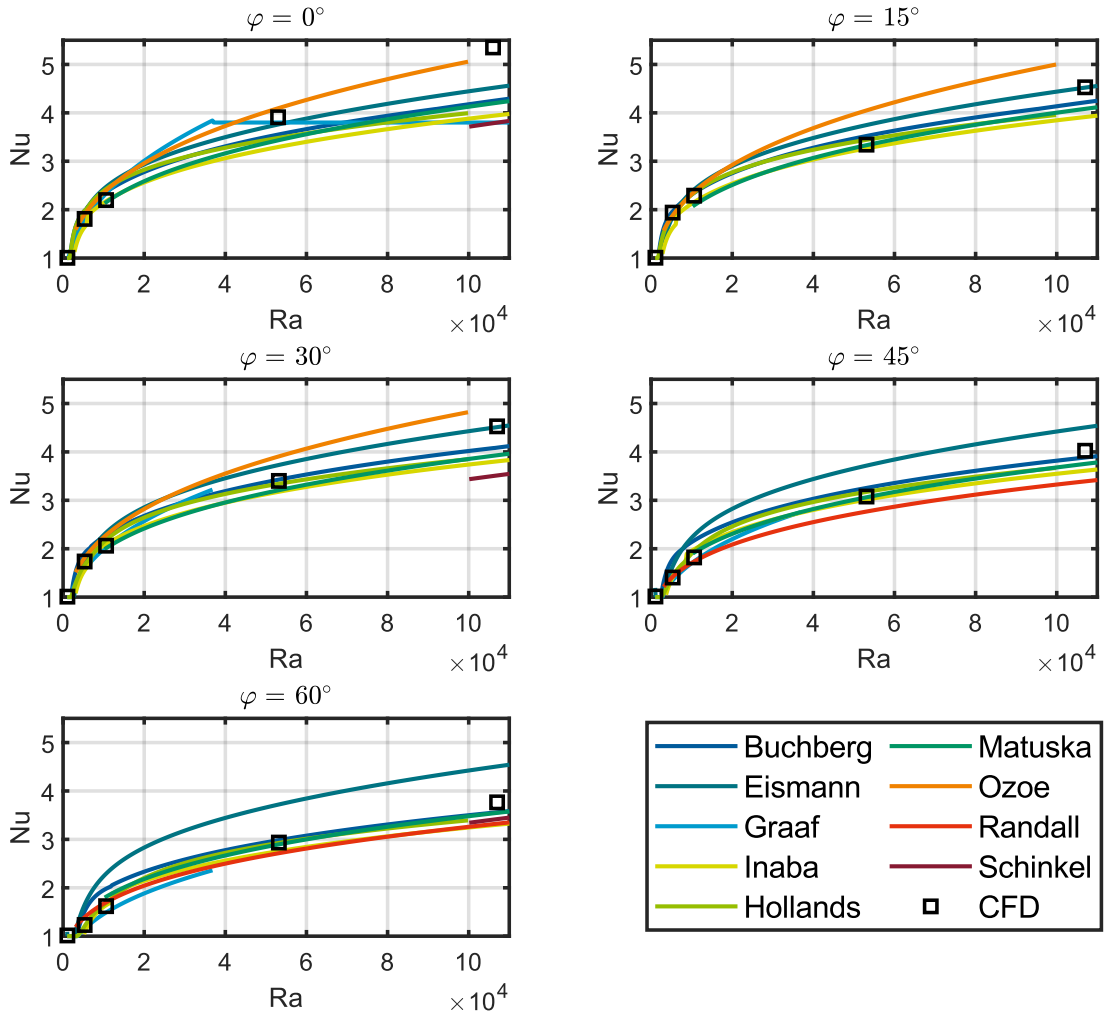

Fig. 2: Validation of the CFD model results (□) with Nusselt correlations (–) from literature for five different inclination angles. The plots show a good fit between the numerical and analytical results.

3.3 Parametric Study

For all sets of parameters, the heat flow rates, material properties, and temperatures have been computed to obtain Nusselt and Rayleigh numbers. For each inclination, the results are shown in Fig. 3. The simulation results indicate similar shaped Nusselt curves as given in the literature. To describe the dependence of Nu and Ra the following expression has been used:

$\mathrm{Nu} = [(1 + (C\ Ra^n)^b)]^{1/b}$ (eq. 4) C, n, b: Parameters for non-linear least square regression

This equation was also used by ElSherbiny (1996) to describe the convective heat transfer for cavities which were heated from above. Fig. 3 shows that this approach can likewise be used to describe the heat transfer for cavities heated from below. A non-linear least square fit has been performed to obtain a set of parameters for eq. 4. The data fits hold coefficients of determination and root-mean-square errors as: $R^2 = \{0.992, 0.994, 0.991, 0.985, 0.983, 0.923\}$ and $RMSE = \{0.184, 0.128, 0.135, 0.158, 0.126, 0.079\}$. This confirms the good fit of the equation for the simulation results.

The derived equations were used to compute the heat transfer coefficients for different widths, inclination angles and temperature differences ΔT for an Argon-filled cavity. Fig. 4 shows contour plots of h with variable cavity widths and temperature levels for the front $\varphi_f = 40°$ and back $\varphi_b = 140°$. Furthermore, the contours for the equations from Hollands et al. (1976) (for the front) and ElSherbiny (1996) (for the back) have been plotted to compare them with the CFD results. It has to be noted, that the empirical correlations are not valid for all aspect ratios which were used for computation. However, these correlations were used to make a comparison possible and show any deviations. White spaces surround the contours as they are capped to the valid Ra and φ ranges of the equations.

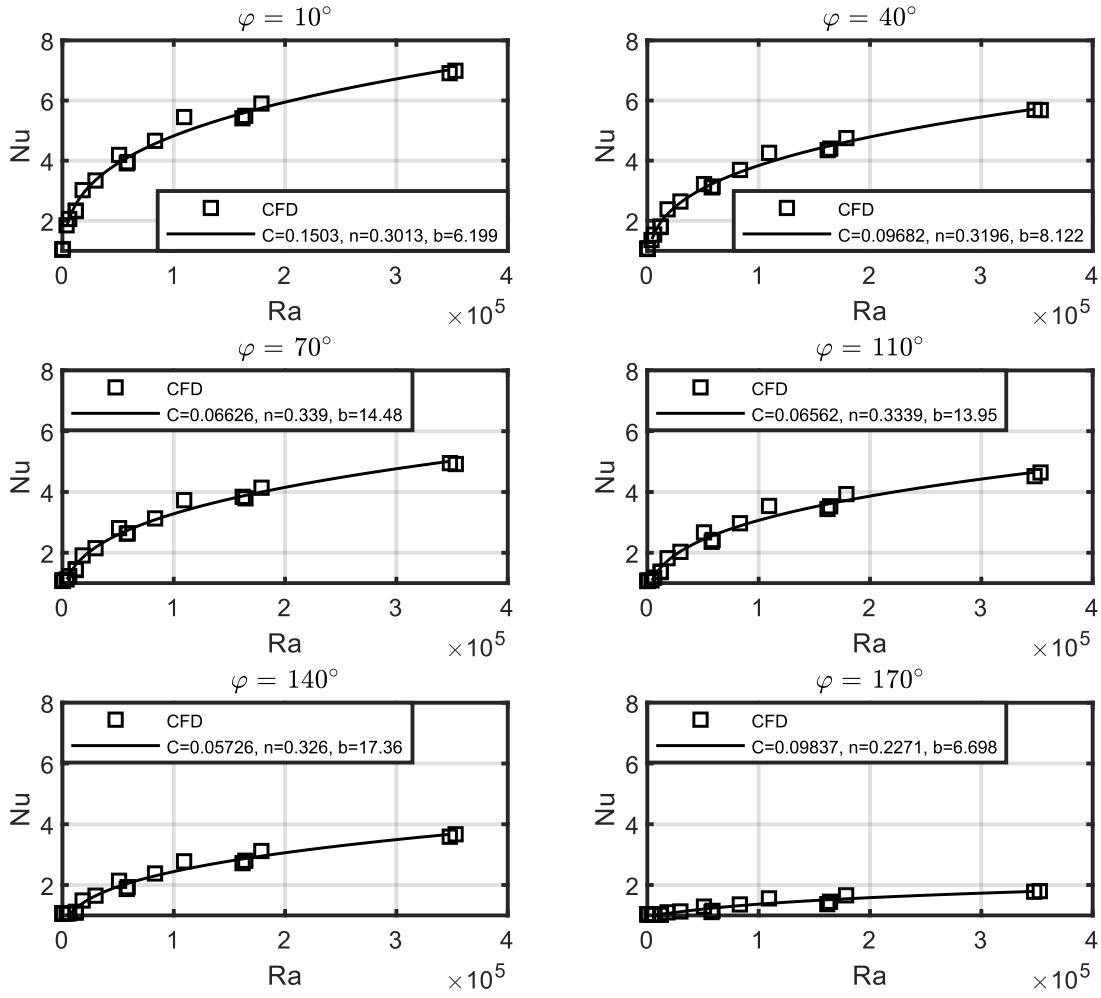

Fig. 3: Nusselt vs. Rayleigh number for six inclination angles (φ). The curves (–) have been determined by a non-linear least square fit. Simulation results (□) were obtained by a parametric study for a typical operation range of IGFPCs.

As expected, there is a difference between the heat transfer at the front and back side of the collector. Hart (1971) has shown that a cavity which is heated from above has a more stable flow regime as compared to the cavity heated from below. This is resulting for both the empirical calculation and the CFD results. It is $h_b < h_f$ in both cases. Moreover, there is a range of W where h rises significantly. If $W < W^* \approx 12$ mm, h increases, whereas for larger widths $\partial h/\partial W < 0$.

A comparison between the empirical and the CFD results at the front cavity shows that for $10 < W < 20$ mm the contours are different. Hollands et al. (1976) equation reveals a local minimum of h for a given ΔT and variable widths. This is not the case for the CFD model. This effect can be explained by the last addend in the correlation of Hollands et al. (1976) which is creating a buckling to the Nu-Ra curve. Hence, the CFD model differs from the empirical solution. The maximum deviation is 25.8 % and the RMS deviation is 0.237 W m^{-2}K^{-1} or 7.3 %. Nevertheless, for both contours, the sensitivity of h to W decreases with increasing values of W. For $\Delta T \approx 35$ K and $W > 20$ mm h becomes nearly independent of W.

When comparing the empirical with the CFD results at the back side cavity, a greater amount of similarity is visible. The maximum deviation is 16.9 % and the RMS deviation is 0.181 W m^{-2}K^{-1} or 9.1 %. The correlations derived from the CFD model show a greater $|\partial h/\partial \Delta T|$ for $W > 20$ mm. Yet, the values of h are in the same order of magnitude for both contours.

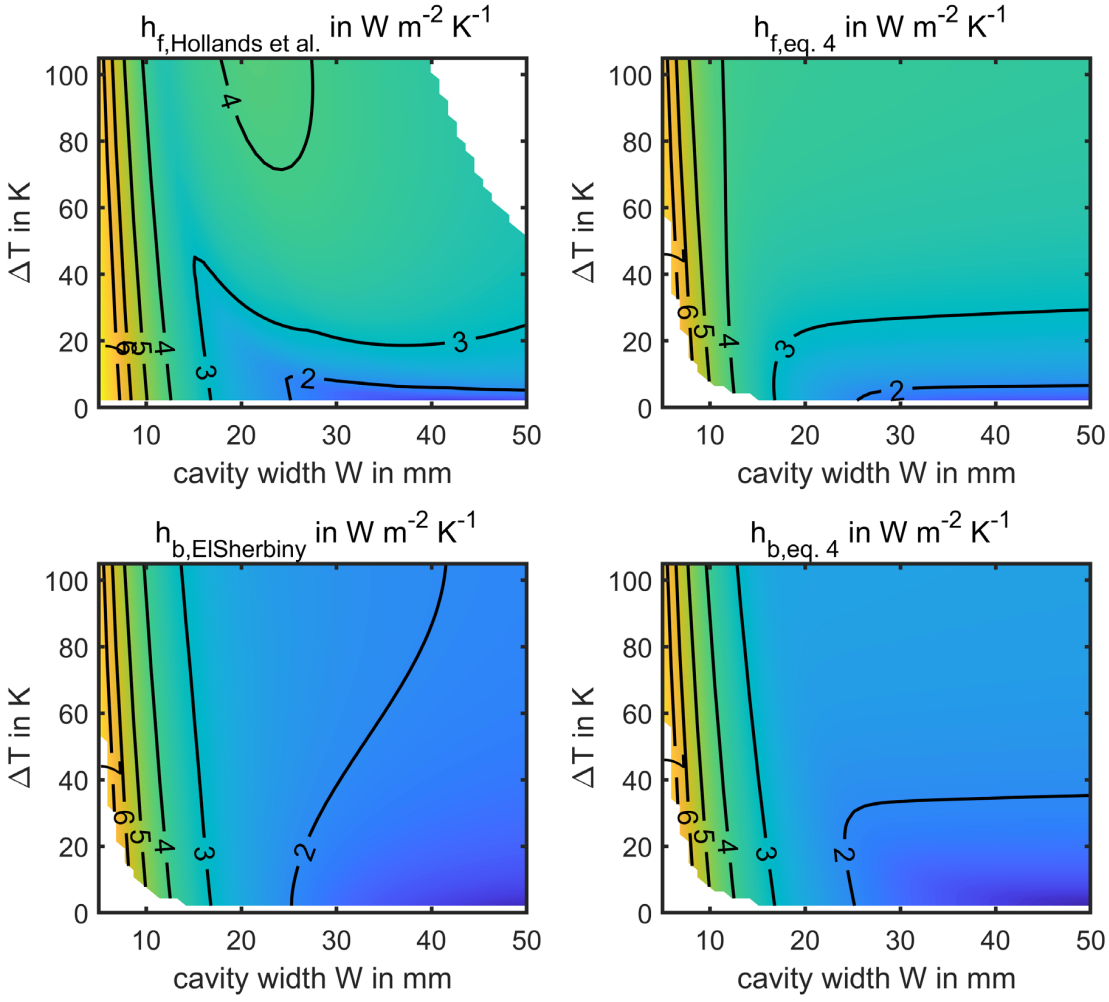

Fig. 4: Contour plot of the convective heat transfer coefficient (h) with respect to variable cavity widths (W) and temperature differences (ΔT). On the left, the Nusselt correlations of Hollands et al. (1976) and ElSherbiny (1996) have been used. On the right, the values were computed using equation 4. The front values (subscript f) are shown for an inclination of 40° and the ones on the back side (subscript b) for 140°. White spaces surround the plots and represent capped areas in which the used equations exceed validity limits for Rayleigh number (Ra) and inclination angle (φ). Argon was considered as the cavity gas.

4. Conclusions

The convective heat transfer inside the enclosed cavity of IGFPCs can partially be computed using Nusselt-Rayleigh number correlations from the literature. An analysis of these equations has shown that their validity range does not cover both high aspect ratios and the entire spectrum of Ra and φ. CFD simulations were used to obtain a new set of correlations which can be used for the entire operating range of IGFPCs. The expression $[(1 + (C\ Ra^n)^b)]^{1/b}$ was found to be precise for describing the Nu-Ra dependence for the following set of inclination angles: $\varphi = \{10,40,70,110,140,170\}$ and this range of Rayleigh numbers: $Ra < 3.2 \times 10^5$. The results confirm that convective losses of IGFPCs occur predominantly at the front side of the collector. For the rear cavity, the flow pattern is subcritical and therefore the losses are smaller for the most parameter sets. On the front side, the heat transfer coefficient h_f is more sensitive to ΔT and W, and thus more sensitive to Ra. This gives substantial evidence, that the absorber position is of significant importance for IGFPCs. Placing it asymmetrically inside the cavity can lead to a performance benefit without having to increase the glass spacing. Consequently, this allows manufacturers to assemble thinner collectors, reduce costs for the edge seal material and thus reduce collector costs.

Overall, the concept of IGFPCs offers potential cost reductions for solar district heating due to its design and production characteristics. The presented study introduced a new set of correlations for describing the convective losses of IGFPCs. Using these equations allows engineers to design IGFPCs with minimized convective losses and to find a balance between material cost (edge seal material) and efficiency (ideal distance between absorber and glass cover). As convective losses represent roughly a third of the overall losses of flat-plate collectors, the influence of design changes on the collector performance can be estimated with the derived equations. However, the equations have not yet been fully validated through comparison with experimental data. Hence, experimental prototype tests are needed in order to confirm the validity of the equations and making them reliable for practical design.

As the aforementioned results focus on the convective heat transfer for the cavity of IGFPCs, there is further research potential on the radiative-convective effects. Another parametric CFD study including radiation allows for findings which demonstrate the share of radiation in the total heat transfer.

5. Acknowledgments

The work presented in this paper was funded by the Federal Ministry of Economic Affairs and Energy of the Federal Republic of Germany within the 7th Energy Research Program under the project “flexLAC” (Project ID 03ETW015-A). The overall aim of “flexLAC” is to design a mass-producible insulated glass flat-plate collector which is able to reduce heat generation costs for solar district heating.

6. References

ANSYS, Inc., 2020. ANSYS Fluent 2020 R2. Build Time: May 29 2020 07:22:43 EDT Build ID: 10176, Canonsburg.

Ayyaswamy, P., Catton, I., 1973. The Boundary-Layer Regime for Natural Convection in a Differentially Heated, Tilted Rectangular Cavity. Journal of Heat Transfer 95 (4), 543–545.

Buchberg, H., Catton, I., Edwards, D.K., 1976. Natural Convection in Enclosed Spaces - A Review of Application to Solar Energy Collection. Journal of Heat Transfer 98 (2), 182–188.

de Graaf, J. G. A., van der Held, E.F.M., 1953. The relation between the heat transfer and the convection phenomena in enclosed plane air layers. Applied Scientific Research 3 (6), 393–409.

Eismann, R., 2015. Accurate analytical modeling of flat plate solar collectors: Extended correlation for convective heat loss across the air gap between absorber and cover plate. Solar Energy 122, 1214–1224.

ElSherbiny, S.M., 1996. Free convection in inclined air layers heated from above. International Journal of Heat and Mass Transfer 39 (18), 3925–3930.

Eurostat, 2018. Disaggregated final energy consumption in households - quantities. https://ec.europa.eu/eurostat/databrowser/view/NRG_D_HHQ__custom_690516/default/table?lang=en. Accessed 16 March 2021.

Giovannetti, F., Kirchner, M., 2015. Performance and Reliability of Insulated Glass Collector Prototypes, in: Conference proceedings / EuroSun 2014, International Conference on Solar Energy and Buildings, Aix-les-Bains, France, 16 - 19 September. Proceedings of the EuroSun 2014 Conference. International Solar Energy Society, Freiburg, Germany, pp. 1–7.

Giovannetti, F., Kirchner, M., Kliem, F., Hoeltje, T., 2014. Development of an Insulated Glass Solar Thermal Collector. Energy Procedia 48, 58–66.

Hart, J.E., 1971. Stability of the flow in a differentially heated inclined box. Journal of Fluid Mechanics 47 (3), 547–576.

Hollands, K.G.T., Unny, T.E., Raithby, G.D., Konicek, L., 1976. Free Convective Heat Transfer Across Inclined Air Layers. Journal of Heat Transfer 98 (2), 189–193.

Inaba, H., 1984. Experimental study of natural convection in an inclined air layer. International Journal of Heat and Mass Transfer 27 (8), 1127–1139.

Leibbrandt, P., Giovannetti, F., Schabbach, T., Jordan, U., 2022. Improved calculation approach of the heat transfer in inclined insulating gas layers. Solar Energy 231, 252–261.

Leibbrandt, P., Schabbach, T., 2020. Optimized Design of the Insulating Gas Layer in Solar Thermal Collectors, in: Proceedings of the ISES EuroSun 2020 Conference – 13th International Conference on Solar Energy for Buildings and Industry, pp. 664–668.

Leibbrandt, P., Schabbach, T., Dölz, M., Rhein, M., 2017. Experimental and CFD Optimization on Flow and Heat Transfer to a Solar Flat-Plate Glass Collector, in: Proceedings of SWC2017/SHC2017. International Solar Energy Society, Freiburg, Germany, pp. 2043–2052.

Matuska, T., Zmrhal, V., 2009. A Mathematical Model and Design Tool "Kolektor 2.2" - Reference Handbook.

Ozoe, H., Sayama, H., Churchill, S.W., 1975. Natural convection in an inclined rectangular channel at various aspect ratios and angles—experimental measurements. International Journal of Heat and Mass Transfer 18 (12), 1425–1431.

Randall, K.R., Mitchell, J.W., El-Wakil, M.M., 1979. Natural Convection Heat Transfer Characteristics of Flat Plate Enclosures. Journal of Heat Transfer 101 (1), 120–125.

Schinkel, W.M.M., 1980. Natural convection in inclined air-filled enclosures, Pijnacker.

Summ, T., Ehrenwirth, M., Trinkl, C., Zörner, W., 2020. Entwicklung eines Großflächenkollektors in Isolierglasbauweise für den Einsatz in Wärmenetzen, in: Online-Symposium Solarthermie und innovative Wärmesysteme. Tagungsunterlagen, pp. 435–448.

Tschopp, D., Tian, Z., Berberich, M., Fan, J., Perers, B., Furbo, S., 2020. Large-scale solar thermal systems in leading countries: A review and comparative study of Denmark, China, Germany and Austria. Applied Energy 270, 114997.

UN Environment Programme, 2020. Renewables 2020 Global Status Report, Paris. https://www.ren21.net. Accessed 14 March 2021.

World Resources Institute, 2019. CAIT Climate Data Explorer - Country Greenhouse Gas Emissions. http://cait.wri.org. Accessed 16 March 2021.

Appendix

Tab. 3: Mesh configurations for validation and parametric study

Property	Symbol	Validation setup	Parametr. study	Unit
Width	W	30	5 – 50	mm
Length	L	1440	2500	mm
Depth	$\frac{D}{2}$	432	750	mm
Cells in x	N_x	500	750	–
Cells in y	N_y	150	225	–
Cells in z	N_z	30	15	–
Cell count	N	2,250,000	2,531,250	–

Tab. 4: Constants for the numerical and analytical analysis

Name	Symbol	Values	Unit
Earth's acceleration	g	9.81	$\mathrm{m\,s^{-2}}$
Roughness glass	κ_{gl}	0.0010	mm
Roughness side walls	κ_w	0.0016	mm
Molar mass Air	M_{Air}	28.959	$\mathrm{kg\,kmol^{-1}}$
Characteristic length Air	σ_{Air}	3.711	Å
Energy parameter Air	ε_{Air}	78.600	K
Degree of freedom Air	f_{Air}	5	–
Molar mass Argon	M_{Argon}	39.948	$\mathrm{kg\,kmol^{-1}}$
Characteristic length Argon	σ_{Argon}	3.542	Å
Energy parameter Argon	ε_{Argon}	93.300	K
Degree of freedom Argon	f_{Argon}	3	–